Available online at www.sciencedirect.com
SCIENCE DIRECT®
Physics Letters A 339 (2005) 497–502
PHYSICS LETTERS A
www.elsevier.com/locate/pla

Microstructure and polarity of epitaxial ZnO films grown on LSAT(111) substrate studied by transmission electron microscopy

Yu-Zi Liu [a,*], M.J. Ying [a], X.L. Du [a,*], Z.Q. Zeng [a], Z.X. Mei [a], J.F. Jia [a], Q.K. Xue [a], Z. Zhang [b]

[a] *Beijing National Laboratory for Condensed Matter Physics, Institute of Physics, Chinese Academy of Sciences, Beijing 100080, China*
[b] *Beijing University of Technology, 100 Pingle Yuan, Chao Yang District, Beijing 100022, China*

Received 23 February 2005; accepted 31 March 2005

Available online 14 April 2005

Communicated by J. Flouquet

Abstract

Transmission electron microscopy is used to investigate the structural characteristics of epitaxial ZnO thin films grown on $(LaAlO_3)_{0.3}(Sr_{0.5}Ta_{0.5}O_3)_{0.7}(111)$ (LSAT) by rf plasma-assisted molecular beam epitaxy. It is found that the growth temperature plays a key role in the formation of microstructures in ZnO film. Growth temperature dependence of rotation domain, interface and dislocation structures is studied, and the mechanism for polarity selection is discussed.

PACS: 61.72.Ff; 73.61.Ga; 68.37.Ef

Keywords: Microstructure; Zinc oxide; TEM

1. Introduction

ZnO is a wurtzite wide band gap ($Eg = 3.37$ eV) semiconductor with large exciton binding energy of 60 meV. Recently, ZnO has attracted much attention in terms of its potential applications in blue and ultraviolet light emitters [1,2]. To prepare high quality ZnO films, various substrates, such as $ScAlMgO_4$ [3], CaF_2 [4], $MgAl_2O_4$ [5], have been used. Since lattice defects, such as threading dislocations, stacking faults and rotation domains, seriously affect the performance of ZnO-based optoelectronic devices, it is of great importance to characterize these defects and develop some techniques to reduce their density.

LSAT is a solid solution between $LaAlO_3$ (LAO) and Sr_2AlTaO_6 (SAT) with a mol ratio of 3/7, which shows a mixed perovskite structure with the same C6 symmetry as wurtzite ZnO along the (111) plane.

* Corresponding authors.
E-mail addresses: yzliu@blem.ac.cn (Y.-Z. Liu), xldu@aphy.iphy.ac.cn (X.L. Du).

0375-9601/$ – see front matter
doi:10.1016/j.physleta.2005.03.081

Therefore, LAST(111) is a good candidate as substrate for ZnO epitaxy, [6] although the lattice mismatch is as large as 19%. No investigations, however, have been performed on the microstructure properties of ZnO film. In this Letter, high resolution transmission electron microscopy (HRTEM) is used to investigate the microstructures and interfaces of the ZnO films on LSAT(111) with different growth temperatures, aiming to understand the role of growth temperature in rotation domain suppression and dislocation reduction. The dislocations in ZnO are studied by dark field images. We also use convergent beam electron diffraction (CBED) to characterize the polarity of the films [7].

2. Experiment

The ZnO films were grown on $(LaAlO_3)_{0.3}(Sr_{0.5}Ta_{0.5}O_3)_{0.7}$(LSAT)(111) by radio frequency plasma-assisted molecular beam epitaxy. The substrates were degreased in trichloroethylene and acetone and rinsed with deionized water before introduced into the load-lock. Then, the substrates were treated by oxygen radicals before the conventional two-step growth of ZnO, i.e., low temperature buffer and high temperature epilayer. Two samples with different buffer-layer growth temperatures were studied. For sample *A*, a thin buffer layer was deposited at 380 °C before the epilayer growth at 620 °C. For sample *B*, the growth temperature of the buffer layer was increased to 500 °C. The HRTEM observations were performed with a Philips CM-200FEG system operating at 200 kV. The specimens were prepared by standard procedures, which include mechanically polishing, dimple grinding, and low angle ion milling.

3. Results and discussion

Rotation domains were observed in the ZnO buffer layer grown at low temperature, which disappear completely when the growth temperature of the buffer layer was increased. Fig. 1(a) shows the cross-section HRTEM images near interface region of sample *A*. Two domains with different in-plane orientations were observed. The azimuth for the left domain is $[10\bar{1}0]_{ZnO}$, whereas the azimuth for the right one is $[11\bar{2}0]_{ZnO}$. Thus, the two domains have an in-plane

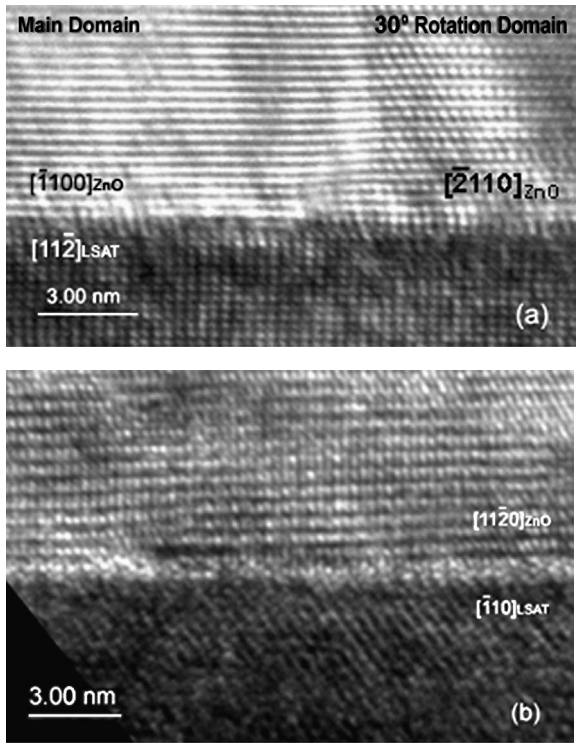

Fig. 1. (a) HRTEM image of sample *A* with the electron beam along [11$\bar{2}$] zone axis of LSAT. Sharp interface and 30° rotation domain are observed. (b) HRTEM image of sample *B* with the electron beam along [11$\bar{2}$0] azimuth of ZnO. The interface is coarse.

30° rotation along [0001]. However, in sample *B*, no rotation domains are observed. Fig. 1(b) shows a typical HRTEM image of this sample. The rotation domain suppression is further confirmed with selected area diffraction pattern (SADP).

Fig. 2(a) shows the SADP taken from the ZnO layer in sample *A*. As indicated by the arrows, two sets of scattering points appear, indicating the coexistence of two kinds of domains. On the other hand, for sample *B* only one set of diffraction pattern is observed (see Fig. 2(c)), suggesting that single domain ZnO film was formed at higher buffer-layer growth temperature. In order to check the crystallographic orientation relationships between ZnO and LSAT, SADP is also taken near interface region in a main domain of sample *A*, the result is shown in Fig. 2(b). The main epitaxial relationship is $(0001)_{ZnO}/\!/(111)_{LSAT}$, and $[11\bar{2}0]_{ZnO}/\!/[\bar{1}10]_{LSAT}$ which is the same as that of sample *B*. From Fig. 2(b), the lattice mismatch be-

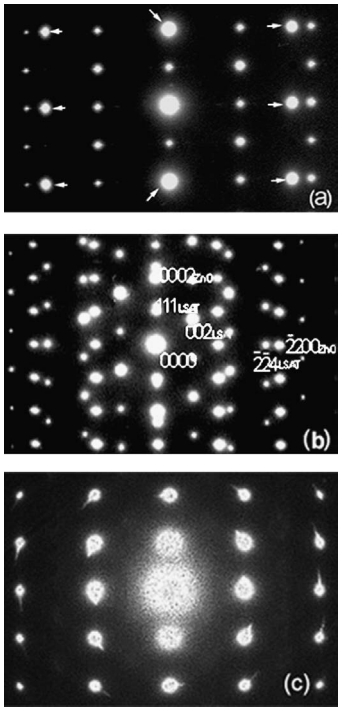

Fig. 2. (a) The SADP near a domain boundary on the ZnO layer showing that there are 30° rotation domains in this film by two sets of points. One is for $[11\bar{2}0]$ zone axis, another is for $[10\bar{1}0]$, as indicated by narrows. (b) Composite SADP of the main domain region in the ZnO epilayer and LSAT substrate of sample A recorded near the interface. The electron beam is parallel to the $[11\bar{2}0]_{\mathrm{ZnO}}$ zone axis. The epitaxial orientation relationship is $(0001)_{\mathrm{ZnO}} /\!/ (111)_{\mathrm{LSAT}}$, $[11\bar{2}0]_{\mathrm{ZnO}} /\!/ [\bar{1}10]_{\mathrm{LSAT}}$, $[\bar{1}100]_{\mathrm{ZnO}} /\!/ [11\bar{2}]_{\mathrm{LSAT}}$. (c) SADP of large area of ZnO film of sample B. In this pattern the spots are slightly arched, indicating the existence of small angle grain boundaries. There is only one set of points indicating a single domain film.

tween ZnO and LSAT substrate is also determined for the main domains in sample A. From the formula

$$D = \left(\frac{1}{R_{2\bar{2}00\mathrm{ZnO}}} - \frac{1}{R_{\bar{2}\bar{2}4\mathrm{LSAT}}} \right) \Big/ \frac{1}{R_{\bar{2}\bar{2}4\mathrm{LSAT}}}$$

(R is the distance between the scattering and transmitted points), the lattice mismatch was measured to be about 19%, in good agreement with the theoretical lattice mismatch between ZnO and LAST. In addition, it should be noticed that in Fig. 2(c), the diffraction spots are slightly arched, indicating the existence of small angle grain boundaries in this film [8].

The structure of rotation domains in sample A is further characterized with dark field images, as shown

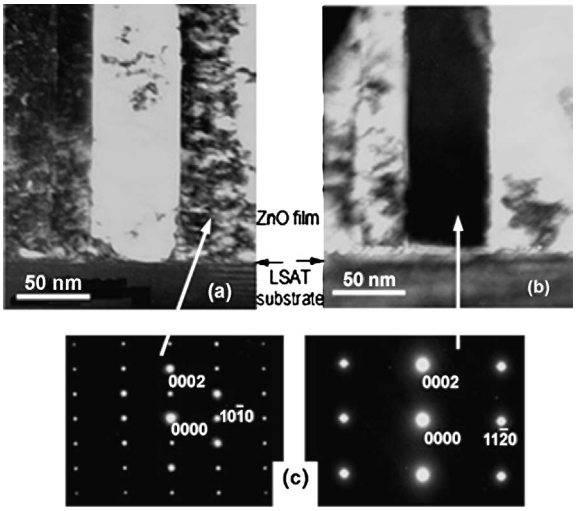

Fig. 3. Dark field images and corresponding SADP taken in sample A. (a) under $g = (11\bar{2}0)$ near $[10\bar{1}0]$ zone axis. (b) Under $g = (10\bar{1}0)$ near $[11\bar{2}0]$ azimuth (c) SADP, identifying that the contrast strips are rotated 300 with each other.

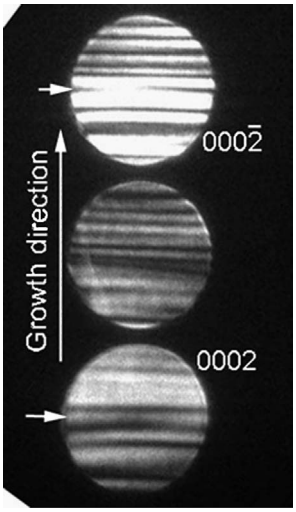

Fig. 4. The CBED pattern of the ZnO film of sample A, indicating an oxygen polarity of ZnO film.

in Fig. 3. Fig. 3(a) was taken under $g = (11\bar{2}0)$ near $[10\bar{1}0]_{\mathrm{ZnO}}$ zone axis, and Fig. 3(b) along $g = (10\bar{1}0)$ near $[11\bar{2}0]_{\mathrm{ZnO}}$ azimuth. We can determine the rotation domain according to the SADP of the contrast strips (Fig. 3(c)). From the contrast, the domain column size is estimated to be ~ 50 nm.

The oxygen polarity of the ZnO film was determined by CBED pattern, as shown in Fig. 4. The

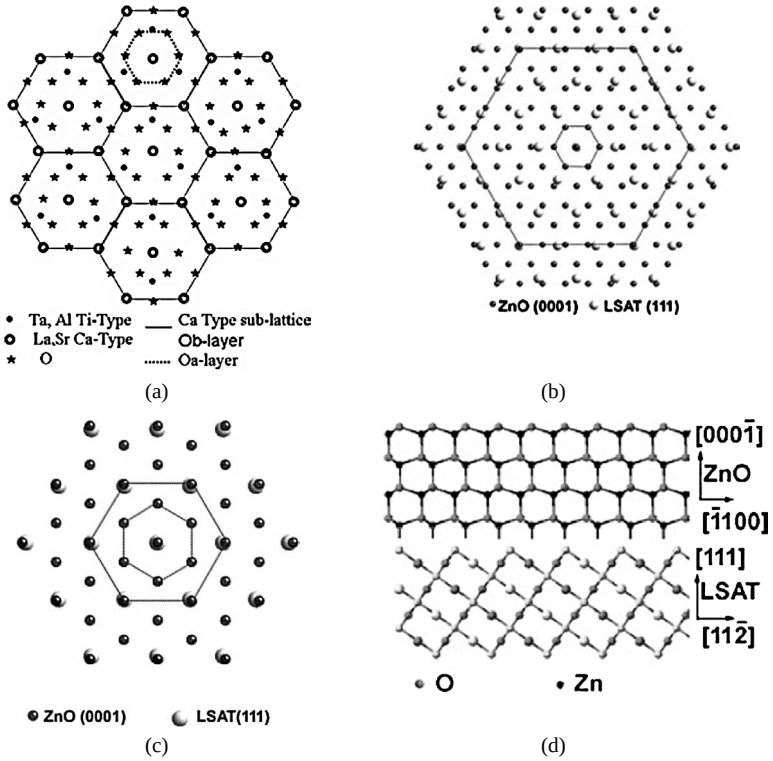

Fig. 5. (a) The schematic viewed in [111] projection. The Ca-type sublattice and the O sublattice are in the same plane while the Ti-type sublattice is about $12^{-1/2}$a (a is the lattice parameter) below the Ca and O sublattice. Two types of hexagons indicate the two O-layers. The dashed hexagon shows the Oa-layer and the large one the Ob-layer which is the same as Ca-type sublattice. (b) The configuration of large lattice-mismatched (18.9%) epitaxial growth of ZnO on O sublattice of LSAT. (c) The configuration of small lattice-mismatch (2.9%) epitaxial growth of ZnO on Ca sublattice. There is 30° rotation between (b) and (c). (d) The schematic diagram of the epitaxial relationships between ZnO and LSAT for sample *B*. The ZnO and LSAT are viewed in the $[11\bar{2}0]$ and $[\bar{1}10]$ projections respectively. And the lattice ratio between ZnO and LSAT is about 5/3.

fringes in the (0000) disk were symmetrical for the electron beam parallel to the (0001) face. If the film is Zn-polarized, the central fringes in the (0002) and $(000\bar{2})$ should appear bright and dark, respectively, because the reflection from the $(0001)_{Zn}$ face is stronger than that of $(000\bar{1})_O$ face [9].

There are steps on the surface of perovskite crystal (111) plane [10]. So, the LSAT(111) plane has two termination surfaces, one is constitutive of coplanar O and Ca-type ions, the other is formed with Ti-type ions only. The epitaxial relationships between ZnO and the substrates are schematically illustrated in Fig. 5. Fig. 5(a) corresponds to the projection of the LSAT(111) plane. The Ca-type and O sublattices are in the same plane, while the Ti-type sublattice is below (or above) the Ca and O sublattice. On oxygen terminated LSAT(111) surface, one dangling bond for each O is expected after the sufficient O-plasma pretreatment. Thus, the outermost surface is formed by two O layers; one is coplanar with Ca-type ions (we call it as 'Oa-layer'); the other (Ob-layer) is the one adsorbed on the Ca-type ions (see Fig. 5(a)). On the other hand, the O layer on the Ti-type surface has the same sublattice as Oa-layer because of the nature of 6-coordination of Ti-type ion in LSAT, e.g., each surface Ti-type ion is bonded with three adsorbed O atoms. Therefore, after oxygen radical treatment, the LSAT(111) surface is consisted of the dominant Oa layer and minor Ob layer.

On such surface, two kinds of in-plane epitaxial relationships between ZnO and LSAT will be formed at low temperature as shown in Fig. 5(b) and (c). Fig. 5(b) is for the case with the Oa layer, which results in the formation of main domains in sample *A*.

The other one (Fig. 5(c)) originates from the Ob layer forming the minor domains. It is very clear that there is in-plane 30° rotation between them. The structure of this kind of 30° rotation domains is quite different from that of 60° rotation domains observed in Pt film grown on $SrTiO_3$(111) reported in Ref. [10]. The 60° rotation domain has a same in-plane orientationship, but a different stacking sequences, i.e., fcc for main domains and fcp for 60° rotation domain [10]. The coexistence of these two stacking sequences is not rare in metal films.

Rotation domains are completely suppressed when the buffer layer growth temperature is increased, which is probably attributed to the desorption of the Ob layer from the Ca-type ions, leaving only one kind of oxygen layer (Oa layer) on LSAT(111) surface. The Ca-type atoms are 12-coordinated in bulk LSAT, 6 in plane, 3 below and 3 above the plane. Therefore, their bonding strength with absorbed oxygen atom is relatively weak when they are at topmost layer. At high temperature, the desorption of the Ob layer is expected to happen. If the deposition rate of ZnO is small at high temperature (in the case of the buffer layer growth for sample *B*), no ZnO nucleus on Ca-type atoms will be formed due to the short adsorption lifetime of oxygen atoms. This assumption is confirmed by the fact that no Zn-polar inversion domains were found in the buffer layer of sample *B*, which will be discussed later. Therefore, we can conclude that the coexistence of the Oa- and Ob-layers at low temperature results in the formation of rotation domains, while at higher temperature, single domain ZnO is achieved due to the desorption of the Ob layer.

Now, we discuss the polarity of the ZnO films. Fig. 5(d) is the projection of the cross section near the interface along ZnO $[11\bar{2}0]$ zone axis. An oxygen terminated LSAT surface with one dangling bond for each O is expected after oxygen plasma pretreatment. When ZnO deposition begins, Zn atoms of the first Zn–O bilayer will bond to the topmost O atoms of LAST, resulting in the O-face of Zn–O bilayer upward, e.g., the O-polar ZnO film, as shown in Fig. 4. On the other hand, Zn-polar domains would be formed if ZnO would nucleate directly on the Ca-type atoms. In this case, O atoms of the first Zn–O bilayer will first form bonds with the topmost Ca-type atoms of LAST. However, this situation does not happen when the growth temperature is high because adsorption lifetime of the oxygen atoms is short. Our TEM also shows no inversion domains in sample *B*.

Fig. 5(d) illustrates that the ratio of lattice distance in ZnO and LSAT is close to 5/3. This domain-matched epitaxy leads to the formation of a large density of misfit dislocations. Fig. 6 shows the dark field cross-section images taken under $g = (11\bar{2}0)$ and $g = (000\bar{2})$ near $[10\bar{1}0]$ azimuth of the ZnO film. Two specimens have almost the same thickness. Therefore, we are able to compare the densities of threading dislocations between them. Many vertical dislocations lines originating from the interface and the threading dislocations through film have been observed along [0001]. The dislocation density at interface is much higher than the upper region. There are three types of threading in hexagonal compact structures, i.e., a-type dislocation (Burgers vector $1/3\langle 11\bar{2}0\rangle$, edge dislocation), a + c-type dislocation (Burgers vector $1/3\langle 11\bar{2}3\rangle$, mixed dislocation), and c-type dislocation (Burgers vector $\langle 0001\rangle$, screw dislocation) [11]. They can be unambiguously characterized by $\{11\bar{2}0\}$ and $(000\bar{2})$ dark field images according to the rule of $g \bullet b = 0$. a-type dislocations are in contrast in the $\{11\bar{2}0\}$ dark field and extinguished in the $(000\bar{2})$ dark field images, c-type dislocation are in contrast in the $(000\bar{2})$ dark field and extinguished in the $\{11\bar{2}0\}$ dark field images. Meanwhile, a + c type dislocations are in contrast in both dark field images. As shown in Fig. 6, there are more edge-dislocations than screw and mixed dislocations. Also no inversion domains exist in sample *A* and sample *B* as no contrast inversions are observed in the two multiple dark field images under the $g = (000\bar{2})$ and $g = (0002)$ with the electron beam along the noncentrosymmetric $[11\bar{2}0]$ axis [12]. We find many strips in Fig. 6(a) and (c) resulting from the small grain boundaries. The density of threading dislocation in upper region of sample *B* is estimated to be approximately $4 \times 10^9/\text{cm}^2$, while in sample *A* it is three times higher. It is well known that the interaction between threading dislocations and the formation of half-loops will reduce the density of threading dislocations in upper region. The half-loops in sample *B* shown in Fig. 6(b) are higher than that in sample *A* (Fig. 6(d)), leading to a lower density of threading dislocations in sample *B*. Therefore, we speculate that higher buffer layer temperature enhances the threading dislocation interactions near the interface, and then more dislocation annihilation and fusion will appear.

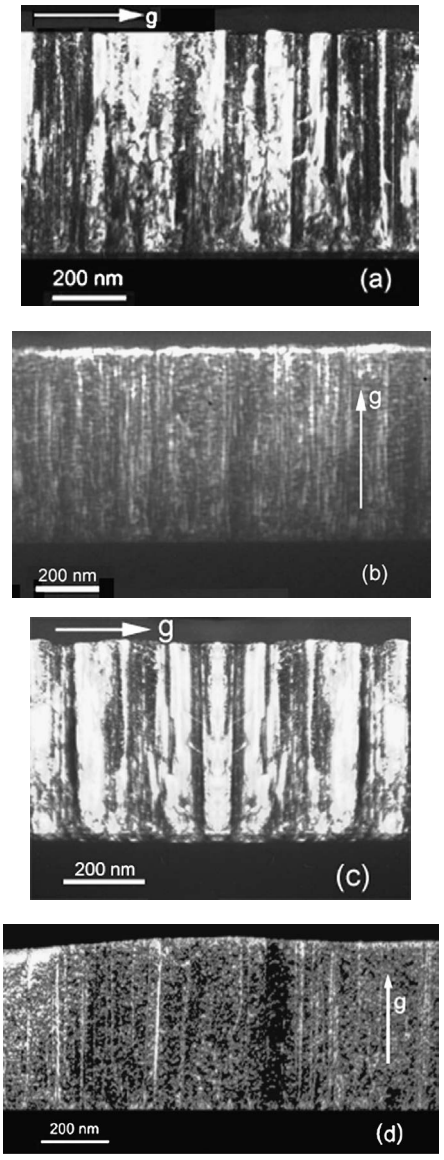

Fig. 6. Dark field cross-section images of ZnO film under reflections $g = (11\bar{2}0)$, (a) and (c) $g = (000\bar{2})$, (b) and (d) near $[10\bar{1}0]$ azimuth. (a) and (b) are performed on sample A, (c) and (d) sample B.

4. Summary

We have used TEM to characterize the microstructure of epitaxial ZnO films on LSAT(111). The crystallographic orientation relationship was determined by SDAP. Defect characterization shows that only threading dislocations exist in our films. From dark field images and HRTEM, 30° rotation domains were observed for ZnO grown at low temperature. They can be suppressed when higher growth temperature for buffer layer is adopted. The oxygen polarity of ZnO films was confirmed by CBED. Although single domain and unipolar ZnO film has been obtained, the defect density is still high because of the large lattice mismatch. Further efforts are still needed for the improvement of the crystal quality.

Acknowledgements

This work is supported by National Science Foundation (60376004, 60476044, 60021403, 10174089) and Ministry of Science and Technology (2002CB613502) of China.

References

[1] D.M. Bagnall, Y.F. Chen, Z. Zhu, T. Yao, S. Koyama, M.Y. Shen, T. Goto, Appl. Phys. Lett. 70 (1997) 2230.
[2] D.M. Bagnall, Y.F. Chen, Z. Zhu, T. Yao, M.Y. Shen, Appl. Phys. Lett. 73 (1998) 1038.
[3] T. Makina, C. Chia, N. Tuan, Y. Segawa, M. Kawasaki, A. Ohtomo, K. Tamura, H. Koinuma, Appl. Phys. Lett. 76 (2000) 3549.
[4] H.J. Ko, Y.F. Chen, J.M. Ko, T. Hanada, Z. Zhu, T. Fukuda, T. Yao, J. Cryst. Growth 207 (1999) 87.
[5] Y.F. Chen, S.K. Hong, H.J. Ko, M. Nakajima, T. Yao, Y. Segawa, Appl. Phys. Lett. 76 (2000) 245.
[6] T. Nakamura, H. Minoura, H. Muto, Thin Solid Films 405 (2002) 109.
[7] B. Dandin, J.L. Rouvière, M. Arlery, Appl. Phys. Lett. 69 (1996) 2480.
[8] Z. Liliental-Weber, H. Sohn, N. Newman, J. Washburn, J. Vac. Sci. Technol. B 13 (4) (1995) 1578.
[9] P. Han, Z. Wang, X.F. Duan, Z. Zhang, Appl. Phys. Lett. 78 (2001) 3974.
[10] A. Asthagiri, C. Niederberger, A.J. Francis, L.M. Porter, P.A. Salvador, D.S. Sholl, Surf. Sci. 537 (2003) 134.
[11] F. Vigué, P. Vennéguès, S. Vézian, M. Laügt, J.-P. Faurie, Appl. Phys. Lett. 79 (2001) 194.
[12] L.T. Romano, J.E. Northrup, M.A. O'Keefe, Appl. Phys. Lett. 69 (1996) 2394.